Open access • Journal Article • DOI:10.1137/0150066

Asymptotic methods for metal oxide semiconductor field effect transistor modeling

Michael J. Ward, F. M. Odeh, D. S. Cohen

Published on: 01 Jun 1990 - Siam Journal on Applied Mathematics (Society for Industrial and Applied Mathematics)

Topics: Method of matched asymptotic expansions, Singular perturbation, Asymptotic expansion and Field-effect transistor

SIAM J. APPL. MATH.
Vol. 50, No. 4, pp. 1099-1125, August 1990

009

ASYMPTOTIC METHODS FOR METAL OXIDE SEMICONDUCTOR FIELD EFFECT TRANSISTOR MODELING*

M. J. WARD†§, F. M. ODEH‡, AND D. S. COHEN†

Abstract. The behavior of metal oxide semiconductor field effect transistors (MOSFETs) with small aspect ratio and large doping levels is analyzed using formal perturbation techniques. Specifically, the influence of interface layers in the potential on the averaged channel conductivity is closely examined. The interface and internal layers that occur in the potential are resolved in the limit of large doping using the method of matched asymptotic expansions. This approach, together with other asymptotic techniques, provides both a pointwise description of the state variables as well as lumped current-voltage relations that vary uniformly across the various bias regimes. These current-voltage relations are derived for a variable doping model respresenting a particular class of devices.

Key words. singular perturbation, interface layer, uniform expansions, current-voltage relations, channel conductivity

AMS(MOS) subject classifications. 35B25, 35B40, 41A60

1. Introduction.

Since its invention in 1960, the metal oxide semiconductor field effect transistor (MOSFET) has been intensely studied, mainly by electronic device engineers, because of its importance in the design of computer memory chips. Initially, rather simplified analytical models were used to determine the lumped current-voltage relations of long-channel devices in various bias regimes. These models were usually derived by means of physical approximations regarding the behavior of the longitudinal electric field—the so-called long-channel approximation—whose range of validity is unclear. Moreover, constant doping density was almost always assumed for the sake of "explicitly solving" the governing equations. Since variable doping implants are often used, especially for moderately short devices and for technological reasons such as the reduction of loss of gate control on channel conductivity, the assumption of constant doping is too severe a restriction. Despite these as well as other shortcomings, these models have proved quite useful in predicting the behavior of long-channel devices and are still extensively employed in circuit simulation packages. Some of the classic papers on analytical MOSFET modeling include [1], [9], and [3]. A comprehensive review of analytical MOSFET modeling is found in [2].

Recently, asymptotic techniques were shown to be an effective tool for investigating the behavior of solutions to the semiconductor equations in many relevant cases. For example, Please [10], using formal asymptotic expansions for large doping levels, constructed the asymptotic potential and provided a detailed description of the I-V characteristics for a one-dimensional forward biased p-n junction. Also Markowich [7], [8], in addition to proving existence and regularity theorems, demonstrated via singular perturbation theory the occurrence of internal and boundary layers in a two-dimensional setting. In this paper we are primarily concerned with resolving the

* Received by the editors September 7, 1988; accepted for publication (in revised form) June 13, 1989. This work was supported by National Science Foundation grant DMS84-00885, United States Army Research Office contract DAAG29-85-K0092, and Air Force Office of Scientific Research grant AFOSR-87-0270.

† Department of Applied Mathematics, California Institute of Technology, 217-50, Pasadena, California 91125.

‡ Mathematical Sciences, I.B.M. Thomas Watson Research Center, Yorktown Heights, New York 10598.

§ Current address, Department of Mathematics, Stanford University, Stanford, California 94305. The work of this author was supported in part by summer internships at IBM and by an IBM Predoctoral Fellowship.

structure of solutions to the governing equations for the MOSFET with small aspect ratio. The asymptotic techniques used are related to [10], but are somewhat more involved due to rapid changes in the potential near the semiconductor-insulator interface. This asymptotic approach offers certain advantages over traditional modeling methods. For example, variable doping density can be easily taken into account and, more importantly, it allows us to compute closed form current-voltage relations that vary uniformly across the various bias regimes. In addition, this approach also provides a pointwise description of the state variables, in contrast to the earlier long-channel models that only determined lumped characteristics. An outline of the paper is given at the end of the following section after the formulation of the mathematical model and a brief introduction to the operation of the MOSFET.

We remark here that the problems associated with the design of very short-channel devices cannot be addressed by analytical long-channel modeling. For these devices, punchthrough between the source and drain becomes a possibility and, perhaps more importantly, the validity of the conventional drift-diffusion model must be more carefully examined. The analysis of these very short-channel devices, which requires a full numerical discretization of the governing semiconductor equations at each bias point, is outside the scope of this paper. An excellent overview of numerical device simulation is presented in Fichtner, Rose, and Bank [4].

2. Mathematical formulation and outline. A cross-sectional view of the MOSFET is shown in Fig. 1. Electrical connections are made to the metal gate electrode and to the n-well reservoirs that comprise the source and drain regions. This device is designated as an n-channel MOSFET, since for appropriate voltage biases the current flow between the source and drain is due to the transport of mobile conduction electrons parallel to the semiconductor-insulator interface. The conductivity of this channel between the source and drain is greatly influenced by the normal component of the electric field established by the voltage applied to the gate. Since the gate is isolated

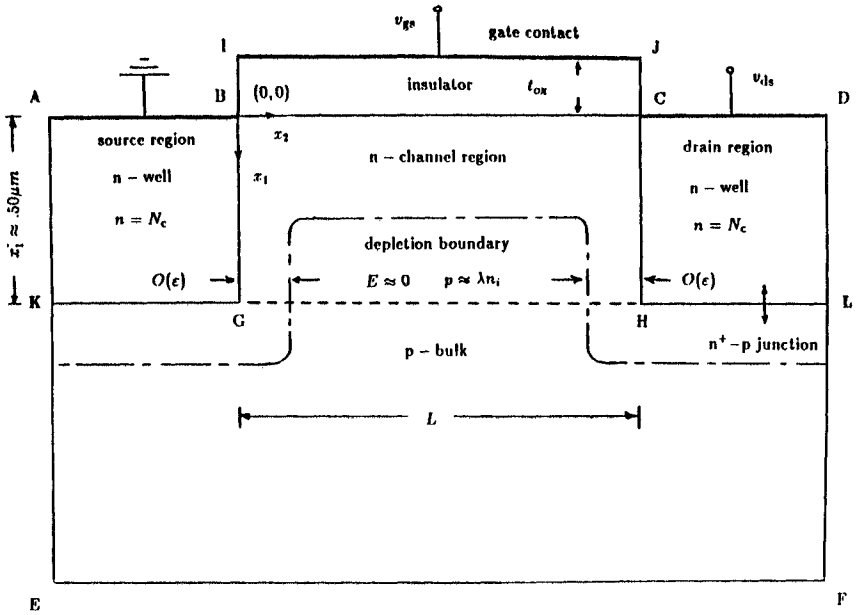

FIG. 1. *Cross-sectional view of the* MOSFET.

from the semiconductor by a layer of insulating material typically made of silicon dioxide, the modulating effect of the gate on the conductivity of the channel is purely by a field-effect mechanism. An electron current between the source and drain then results from applying a bias between the source and drain contacts. One of the primary goals of "analytical" modeling is to determine the amount of this current flow as an "explicit" function of the source-drain bias for various ranges of gate voltage. These current-voltage relations are called I-V characteristics.

The migration of the conduction electrons parallel to the interface can be a result of both drift, under the influence of the electric field, and diffusion due to concentration gradients. The asymptotic analysis presented below delineates the ranges of gate and source-drain bias for which the electron current density is dominated by either the drift or diffusion component.

In general, the MOSFET is a four terminal device with voltages applied to the gate, source, drain, and substrate. Without loss of generality, we assume that the substrate and the source are kept at the same voltage. Allowing for a source-substrate bias simply introduces another parameter into the model and does not affect the structure of solutions to the governing equations. All voltage quantities are referenced with respect to the source.

To simplify the geometry, the semiconductor equations will be solved in the rectangular region BGHC. However, since the behavior of the current-voltage relations depends strongly on the electric field occurring in the insulator, we must solve for the electrostatic potential in the oxide IBCJ. The equations in the semiconductor and the oxide are then coupled through the boundary conditions to be imposed on the semiconductor-insulator interface BC. We now introduce the relevant equations and the associated boundary conditions.

In the region BGHC, the equations comprising the static drift-diffusion model for an n-channel MOSFET, assuming no recombination and that holes remain in thermal equilibrium, are

$$\begin{aligned} &\varepsilon_s \nabla \cdot \mathbf{E} = -\rho \equiv q(p - n + N), \\ &\mathbf{J}_n = q\mu_n\left(\frac{kT}{q}\nabla n + n\mathbf{E}\right), \\ &\nabla \cdot \mathbf{J}_n = 0, \\ &\nabla \psi = -\mathbf{E}, \\ &p = n_i\, e^{-q\psi - kT}, \end{aligned} \tag{2.1}$$

where

n, p	are the electron and hole concentrations,
N	is the concentration of selected impurities or dopants,
$\mathbf{J}_n$	is the electron current density,
$\mathbf{E}, \psi$	are the electric field and electrostatic potential,
μ_n	is the electron mobility,
ε_s	is the dielectric constant of the semiconducting material,
ρ	is the space charge density,
n_i	is the intrinsic carrier concentration,
q	is the charge of a proton,
k	is the Boltzmann's constant,
T	is the assumed constant lattice temperature.

The combination kT/q is called the thermal voltage v_{th}.

The main assumptions of the model are that the holes remain in equilibrium and that there is no recombination or generation. For the range of gate voltages to be considered, the hole concentration in the channel region is negligible. Therefore, the current density due to holes in the channel region can be neglected. Thus, the channel current is due, almost exclusively, to the migration of conduction electrons near the interface along the channel. However, any modeling of bulk currents deep in the substrate, where the hole population is large, would have to take into account the hole current density. Assuming that the length scale as a result of the electron carrier lifetime is sufficiently long compared to the channel length, recombination from a Shockley-Read-Hall process can be neglected. In addition, since the fields encountered will only be moderate, we can neglect any generation effects caused by avalanche multiplication. These assumptions on the generation and recombination terms, which result in a divergence free electron current density, are commonly used in analytical MOSFET modeling (see [2]).

The electrical behavior of a semiconductor device is greatly influenced by the spatial distribution of selected impurities, called dopants, that are implanted into the channel to enhance the conductivity. The net impurity concentration, N, is assumed to be completely ionized and does not contribute to the flow of current. Moreover, the doping profile in the active region BGHC, used to enhance the channel conductivity, is assumed to be of the form $N = N(x_1)$. Both the impurity profile in the channel and the mobility model, which may depend on the field, are assumed to be given. The range of validity and the physical justification of this model is discussed in Selberherr [11].

The boundaries of real devices are composed of both physical boundaries, which include contacts and insulating segments, and artificial boundaries needed for numerical and analytical simulations. We now prescribe the boundary conditions for the simplified geometry BGHC.

Neglecting any surface or bulk recombination effects we assume that there is no flux of carriers normal to the interface BC or across the artificial line segment GH. Namely,

$$\mathbf{J}_n \cdot \hat{\eta} = 0 \quad \text{on} \quad x_1 = 0 \quad \text{and} \quad x_1 = x_1^*,$$

where $\hat{\eta}$ is the unit normal to BC and GH and x_1^* is the depth of the n-well reservoirs. Furthermore, assuming no interface charges, the electrostatic potential and the electric displacement vector are continuous across the interface BC

$$\psi|_{sem} = \psi|_{ins} \quad \text{and} \quad \varepsilon_s \frac{\partial \psi}{\partial x_1}\bigg|_{sem} = \varepsilon_i \frac{\partial \psi}{\partial x_1}\bigg|_{ins},$$

where ε_s and ε_i are the dielectric constants of the semiconductor and the oxide, respectively. Neglecting interface charges is not restrictive since their inclusion simply introduces another additive parameter into the model. The boundary condition for the potential on the line segment GH is prescribed later.

The n-well reservoirs of conduction electrons are formed by implanting large concentrations of donor impurities into the semiconducting material. The dopant concentration $N = N_c$ in these two reservoirs, bounded by the rectangular regions ABGK and CDLH, is taken to be constant.

Assuming perfect ohmic contacts for the source and drain AB and CD, this then specifies Dirichlet boundary conditions for ψ and n on the contacts in terms of N_c (see Selberherr [11]). In terms of the simplified geometry BGHC, these boundary conditions, normally imposed on the source and drain, are imposed on BG and CH,

respectively. These boundary conditions, derived from assuming thermal equilibrium and a vanishing space charge on the contacts, are

$$n = \tfrac{1}{2}(N_c + \sqrt{N_c^2 + 4n_i^2}) \sim N_c \quad \text{on BG and CH},$$

$$\psi = v_{th} \ln\left(\frac{N_c + \sqrt{N_c^2 + 4n_i^2}}{2n_i}\right) \sim v_{th} \ln \frac{N_c}{n_i} \quad \text{on source BG},$$

$$\psi = v_{th} \ln\left(\frac{N_c + \sqrt{N_c^2 + 4n_i^2}}{2n_i}\right) + v_{ds} \sim v_{th} \ln \frac{N_c}{n_i} + v_{ds} \quad \text{on drain CH},$$

for $N_c/n_i \gg 1$. Typically $N_c/n_i \approx 10^8$. The difference in the applied bias between the source and drain, v_{ds}, is called the source-drain bias.

The oxide bounded by IBCJ is assumed to be charge neutral and thus in this region the electrostatic potential satisfies

$$\nabla^2 \psi = 0.$$

There is no transport equation for the mobile electrons in the oxide. The boundary condition for the potential on the gate contact IJ is

$$\psi = v_{gs} - v_{fb},$$

where v_{gs} is the externally applied gate bias referenced with respect to the source. The voltage v_{fb} is the flatband voltage, which measures the difference in the work functions between the metal gate and the semiconductor. The boundary conditions on the artificial boundary segments IB and JC are taken to be $\mathbf{E} \cdot \hat{\eta} = 0$.

To begin the analysis we introduce an appropriate scaling of the drift-diffusion model. For MOSFETs, the ratio of the maximum channel dopant concentration to the intrinsic level n_i is normally very large. Therefore, we introduce a large parameter λ by

$$\lambda = \max |N(x_1)/n_i|.$$

However, for $\lambda \gg 1$ rapid variations in the potential normal to the semiconductor-insulator occur. From an analysis of the one-dimensional Poisson equation, these variations occur on a scale of $O((\ln \lambda/\lambda)^{1/2})$. In addition, the electron concentration can range over many orders of magnitude. To normalize the electron concentration, a new independent variable is introduced that has a much smaller range. Also, in terms of this variable, the no-flux boundary condition on the current density vector becomes a pure Neumann condition. Thus, we consider the following scaled variables

$$\begin{aligned} &\psi = v_{th} \ln \lambda \, w, \\ &x_1 = L_d \left(\frac{\ln \lambda}{\lambda}\right)^{1/2} x \quad \text{where } L_d = \left(\frac{kT\varepsilon_s}{n_i q^2}\right)^{1/2}, \\ &x_2 = Ly, \\ &n = n_i e^{(w-\phi)\ln \lambda}, \\ &\mu_n = \mu_c \mu, \end{aligned} \tag{2.2}$$

where ϕ is called the electron quasi-Fermi potential and measures the departure from thermal electronic equilibrium. The physical length scale L_d is called the intrinsic Debye length, and μ_c represents a typical magnitude of the mobility.

With this scaling, the governing equations (2.1) become

$$\tilde{\nabla}^2 w = \frac{1}{\lambda}\left(e^{(w-\phi)\ln\lambda} - e^{-w\ln\lambda}\right) + d(x), \tag{2.3a}$$

$$\tilde{\nabla}^2\phi + \tilde{\nabla}\phi \cdot \left(\frac{\tilde{\nabla}\mu}{\mu} + \ln\lambda\,\tilde{\nabla}(w-\phi)\right) = 0, \tag{2.3b}$$

$$\mathbf{J}_n \equiv (J_{nx_1}, J_{nx_2}) = -\frac{kTn_i\mu_c}{L_d}(\lambda\ln\lambda)^{1/2}\mu\, e^{(w-\phi)\ln\lambda}\tilde{\nabla}\phi, \tag{2.3c}$$

where the normalized doping profile $d(x)$ is defined by

$$d(x) = -\frac{N(L_d(\ln\lambda/\lambda)^{1/2}x)}{n_i\lambda} = O(1) \quad \text{with } d(\infty) = \beta > 0,$$

and the gradient operator in the new variables is

$$\tilde{\nabla} \equiv \left(\frac{\partial}{\partial x}, \varepsilon\frac{\partial}{\partial y}\right) \quad \text{where } \varepsilon = \frac{L_d}{L}\sqrt{\frac{\ln\lambda}{\lambda}}.$$

From this scaling the validity of any one-dimensional analysis normal to the interface is seen to be restricted to channel lengths and maximum dopant concentrations satisfying $\varepsilon \ll 1$. The numerical value of ε for silicon at room temperature with $\lambda = 10^6$, $L_d = 33$ microns and $L = 10$ microns is $\varepsilon \approx .012$. Enforcing the conservative condition $\varepsilon \leqq .01$, we expect that a quasi-one-dimensional analysis in the middle channel region away from the source and drain should be quite adequate for 10 micron or longer devices. For micron and submicron devices with the same channel doping, the governing equations are fully two-dimensional and numerical methods must be employed to accurately solve for the potential.

As a remark, since the voltage quantities are scaled with respect to the thermal voltage, the influence of large source-drain biases that can effect the validity of any one-dimensional approximation is not immediately apparent. Physically, even for $\varepsilon \ll 1$, a large source-drain bias of ≈ 5 volts can cause the device to exhibit significant two-dimensional behavior in the drain end of the channel. The increased influence of the region near the drain for large source-drain biases leads to the physical effect of channel length modulation, which we do not consider, where the current depends on the source-drain bias in a complicated way.

In terms of the electron quasi-Fermi potential, the boundary conditions prescribed above for ψ and n in the scaled domain BGHC transform under (2.2) to

$$\phi = 0 \quad \text{on } y = 0 \quad \text{and} \quad \phi = \frac{\bar{v}_{ds}}{\ln\lambda} \quad \text{on } y = 1, \tag{2.4a}$$

$$\frac{\partial\phi}{\partial x} = 0 \quad \text{on } x = 0 \quad \text{and} \quad \frac{\partial\phi}{\partial x} = 0 \quad \text{on } x = x^*, \tag{2.4b}$$

where $\bar{v}_{ds} = v_{ds}/v_{th}$ and x^* is the scaled depth of the n-well reservoir. The no-flux boundary condition on ϕ imposed at x^* is reasonable since variations in the electric field in the x direction occur on a scale of $\approx .10$ microns for $\lambda = 10^6$, whereas the depth of the source and drain wells is $\approx .50$ microns. This fact implies that an asymptotic boundary condition for the potential along GH is appropriate. The precise value of x^* is not important since the mobile electrons are normally concentrated only near

the interface. In addition, the boundary conditions corresponding to BG and CH for the scaled potential, w, are

$$w = w_{bi} \equiv \frac{\ln (N_c/n_i)}{\ln \lambda} \quad \text{on } y = 0, \tag{2.5a}$$

$$w = w_{bi} + \frac{\bar{v}_{ds}}{\ln \lambda} \quad \text{on } y = 1. \tag{2.5b}$$

To proceed analytically, the potential in the insulator must be modeled. Since the typical oxide thickness, t_{ox}, is approximately .025 microns, we have $d \equiv t_{ox}/L \leqq .01 \ll 1$ assuming $L \approx 10$ microns. Therefore with $d = O(\varepsilon)$ a one-dimensional potential drop in the middle region of the oxide, $y/\varepsilon \gg 1$ and $(1-y)/\varepsilon \gg 1$, is assumed. With this assumption, and using the continuity of the potential and the electric displacement vector across the interface, we obtain the boundary condition

$$-\frac{\partial w}{\partial x} + c_{ox}\sqrt{\frac{\ln \lambda}{\lambda}}\,(w_s + 1) = c_{ox}\sqrt{\frac{\ln \lambda}{\lambda}}\,\frac{\bar{v}_{gs}}{\ln \lambda} \quad \text{on } x = 0 \tag{2.6}$$

for $y/\varepsilon \gg 1$ and $(1-y)/\varepsilon \gg 1$. For convenience in (2.6), we have defined an effective gate voltage, $\bar{v}_{gs}$, by $\bar{v}_{gs} = (v_{gs} - v_{fb} + \ln \lambda)/v_{th}$. This normalization implies that for $\bar{v}_{gs} = 0$ we have $w_s \approx -1$. Using the material constants for silicon and silicon dioxide and taking $t_{ox} = .025$, $L = 10$ microns, the scaled oxide capacitance, c_{ox}, defined by $c_{ox} = \varepsilon_i L_d / t_{ox} \varepsilon_s$ is approximately 450. The value $c_{ox} = 450.0$ is used in all the calculations below.

Using (2.6) as a boundary condition for ψ in the semiconductor region BGHC will determine the surface potential $w(x, 0) \equiv w_s(y)$ and hence the field in the middle region of the oxide. In several special cases, the surface potential will be found to be essentially constant in the middle channel region away from the source and drain.

As a remark, since the potential within an $O(\varepsilon)$ extent of the source and drain BG and CH, respectively, will not be found, an equation that determines the surface potential along the full extent of the interface is not needed. Some models used for the surface potential near the source and drain, which bypass having to solve Laplace's equation for the potential in the oxide, are provided in Greenfield [5].

Finally, in order to derive the I-V characteristics, we need a definition of the source-drain current I_{ds}. Integrating the current density component parallel to the interface over the active channel cross section, we arrive at the definition of the current

$$I_{ds} = -\int_0^{x_1^*} J_{nx_2}\, dx_1. \tag{2.7}$$

Owing to the no-flux conditions (2.4a), (2.4b), we have that I_{ds} is constant with respect to channel-wise direction. Under a more general situation in which recombination currents at the interface are taken into account, an additional averaging of (2.7) over the channel length would have to be done.

In the above expression we have assumed a unit width perpendicular to the plane of the MOSFET. Using the expression for J_{nx_2} from (2.3c), the above equation now reads

$$I_{ds} = I_c \int_0^{x^*} \ln \lambda \frac{\partial \phi}{\partial y}\, \mu \left(\frac{\ln \lambda}{\lambda}\right)^{1/2} e^{(w-\phi)\ln \lambda}\, dx, \tag{2.8}$$

where $I_c = kTn_i\mu_c L_d / L$.

An outline of the remainder of this paper is as follows. In § 3, the equations relating the potential and the quasi-Fermi potential in the middle channel region are obtained by means of a regular perturbation expansion in the aspect ratio ε. This

middle region $O(\varepsilon) \ll y \ll 1 - O(\varepsilon)$, away from the source and drain, is referred to as the mid-channel or outer ε region. In § 4, the equilibrium potential in the outer region is resolved using the method of matched asymptotic expansions (see Kervorkian and Cole [6]) in the large doping limit $\lambda \gg 1$. Here, we analyze the different regimes of behavior of the potential, depending on the value of the gate voltage, with special emphasis on the rather delicate *inversion regime* when the potential varies extremely rapidly near the silicon-oxide interface. Then, the mobile charge in equilibrium is found using standard techniques in the asymptotic evaluation of integrals. In §§ 5 and 6, we combine a discussion of the behavior of the quasi-Fermi potential together with the results of § 4 to obtain the current-voltage relations in the relevant operating regimes for both constant and variable doping. Also, as a by-product, we give a more precise description of the so-called *pinchoff* behavior.

3. The outer ε expansion in the mid-channel region. In the mid-channel region we assume a regular expansion for the electron quasi-Fermi potential and the potential in the form

$$w(x, y) = w^0(x, y) + \varepsilon^2 w^1(x, y) + \cdots,$$

$$\phi(x, y) = \phi^0(x, y) + \varepsilon^2 \phi^1(x, y) + \cdots.$$

In addition, we assume that the mobility model is a known function of both x and the partial derivative in the channel-wise direction of the electron quasi-Fermi potential

$$\mu = \mu\left(x, \frac{\partial \phi^0}{\partial y}\right) > 0.$$

Substituting this expansion into (2.3a), (2,3b), and equating powers of ε yields, to leading order,

$$\frac{\partial^2 w^0}{\partial x^2} = \frac{1}{\lambda}\left(e^{(w^0-\phi^0)\ln\lambda} - e^{-w^0\ln\lambda}\right) + d(x), \tag{3.1a}$$

$$\frac{\partial^2 \phi^0}{\partial x^2} + \left(\frac{1}{\mu}\frac{\partial \mu}{\partial x} + \ln\lambda\left(\frac{\partial w^0}{\partial x} - \frac{\partial \phi^0}{\partial x}\right)\right)\frac{\partial \phi^0}{\partial x} = 0. \tag{3.1b}$$

The no-flux boundary conditions on ϕ, (2.4b), effectively uncouples this leading order system and enforces $\phi^0 \equiv \phi^0(y)$ only, which means that the flow of current is directed primarily parallel to the interface. Using this form, the second-order equation in the expansion of the electron transport equation now reads

$$\frac{\partial^2 \phi^1}{\partial x^2} + \left(\frac{1}{\mu}\frac{\partial \mu}{\partial x} + \ln\lambda\frac{\partial w^0}{\partial x}\right)\frac{\partial \phi^1}{\partial x} = -\left[\phi^{\prime\prime 0} + \left(\frac{1}{\mu}\frac{\partial \mu}{\partial y} + \ln\lambda\left(\frac{\partial w^0}{\partial y} - \phi^{\prime 0}\right)\right)\phi^{\prime 0}\right], \tag{3.2}$$

where the primes denote total derivatives with respect to y. From (3.2) we observe that the second-order equation for ϕ requires knowledge of only the leading order potential.

From the Fredholm alternative, the solvability condition for (3.2) with no flux boundary conditions on $x = 0$ and $x = x^*$ provides the differential equation satisfied by ϕ^0. Integrating (3.2) once and satisfying the required no-flux boundary conditions enforces

$$\phi^{\prime\prime 0} - \ln\lambda(\phi^{\prime 0})^2 + \phi^{\prime 0}\frac{\partial}{\partial y}\ln\left(\int_0^{x^*} \mu(\zeta, \phi^{\prime 0})\, e^{w^0(\zeta,\phi^0)\ln\lambda}\, d\zeta\right) = 0, \tag{3.3}$$

where in general the potential depends on ϕ^0 from (3.1a). This equation can also be written compactly in the form

$$\phi'^0 + \frac{\partial}{\partial y}(\ln(\sigma_m))\phi'^0 = 0 \tag{3.4}$$

where

$$\sigma_m = \sigma_m(x^*, w_s, \phi^0, \phi'^0) \equiv \int_0^{x^*} \mu(\zeta, \phi'^0)\, e^{(w^0(\zeta,\phi^0)-\phi^0)\ln\lambda}\, d\zeta,$$

is the averaged channel conductivity per unit charge. As will be seen in § 5, the first form of the equation for ϕ^0, (3.3), is advantageous for determining the diffusion current in subthreshold gate bias regimes. Integrating (3.4) once shows that $\sigma_m\phi'^0$ is constant in y and comparing it to (2.8) gives

$$\phi'^0\sigma_m(x^*, w_s, \phi^0, \phi'^0)\ln\lambda = \frac{I_{ds}}{I_c}\left(\frac{\lambda}{\ln\lambda}\right)^{1/2} \quad \text{as } \varepsilon \to 0. \tag{3.5}$$

Satisfying the boundary conditions (2.4a) for ϕ^0 at $y=0$ and $y=1$ will thus determine the source-drain current. From (3.5), it is clear that since $v_{ds} > 0$ we must have $\phi^0 \geqq 0$ and that ϕ^0 vanishes identically if $\bar{v}_{ds} = 0$.

In the special case for which $\mu = \mu(\phi'^0)$ only, the source-drain current from (3.5) can be written compactly as

$$I_{ds} \sim -I_c \int_0^1 \mu\phi'^0 Q_c(\phi^0(y))\ln\lambda\, dy \quad \text{as } \varepsilon \to 0, \tag{3.6}$$

where

$$Q_c(\phi^0(y)) = -\left(\frac{\ln\lambda}{\lambda}\right)^{1/2} \int_0^{x^*} e^{(w^0-\phi^0(y))\ln\lambda}\, dx \tag{3.7}$$

is the amount of mobile charge in the channel under nonequilibrium conditions. In § 4, we shall evaluate Q_c asymptotically as $\lambda \to \infty$ in various gate bias regimes.

We now make a few remarks concerning the above perturbation approach to current flow in MOS devices. First, from (3.2), we note that there can be some current flow normal to the interface near the drain end of the channel. In prior modeling, the current flow in the channel away from the source and drain is assumed to be entirely tangential. In fact, (3.4), (3.2), and some algebra show that the current density normal to the interface in the original variables is

$$J_{nx_1} = \frac{I_{ds}}{L}\frac{\partial}{\partial y}\left(\frac{\sigma_m(x, w_s, \phi^0, \phi'^0)}{\phi_m(x^*, w_s, \phi^0, \phi'^0)}\right). \tag{3.8}$$

Second, to determine the I-V characteristics associated with various gate bias regimes and doping profiles, the outer ε equation for the potential w^0 parameterized by ϕ^0 must be solved and the averaged channel conductivity computed. Unfortunately, it is not possible to solve (3.1a) explicitly. However, the outer ε potential can be resolved asymptotically by the method of matched asymptotic expansions in the limit of large doping, $\lambda \gg 1$, for various classes of implant profiles $d(x)$. Using these asymptotic expansions for the potential, the averaged channel conductivity can then be evaluated asymptotically for given mobility models using well known techniques in the asymptotic evaluation of integrals. Furthermore, from the $\lambda \gg 1$ expansion, a pointwise description of the field quantities and the current density vector is available.

Third, the boundary conditions associated with (3.4) on the outer solution are (2.4a). In contrast to the potential, boundary layers in ϕ are not anticipated near the source and drain. However, the use of (3.5) necessitates computing the potential in the *inner* regions near the source and drain in order to determine the I-V characteristics. Since the potential is not analytically known near the source and drain, even for large doping, numerical methods must be employed to compute the potential in these regions and to match to the behavior in the mid-channel region.

In conventional modeling the boundary conditions (2.4a), (2.4b) are used and the potential near the source and drain is neglected. It has been noted by Brews [2] that with this simplification the source-drain bias is not the bias applied on the drain contact but rather should be interpreted as the bias at an $O(\varepsilon)$ distance away from the drain. Using the results of the $\lambda \gg 1$ asymptotics for the outer potential, and adhering to Brews interpretation, we will find closed form expression for the I-V curves in the relevant bias regimes. The influence of the potential in the inner regions on the current flow is currently under investigation.

4. One-dimensional equilibrium potential $\lambda \gg 1$. In this section the potential in the mid-channel region, under the assumption of equilibrium, $\phi^0 \equiv 0$, is analyzed in the limit $\lambda \gg 1$. The asymptotic potential is constructed for a particular class of impurity profile $d(x)$. The results of this section are then easily generalized to nonequilibrium conditions since $\phi^0 \equiv \phi^0(y)$ only.

The class of MOS devices that we are concerned with in this paper are formed by implanting only acceptor impurities, such as boron, into the substrate. The doping profile for these devices in the mid-channel region is modeled by

$$d(x) = \beta + (1-\beta)\, e^{-(x/\sigma)^2} \quad \text{with } 0 < \beta \leqq 1,$$

where β is independent of λ. Typically, $\beta \in [.01, 1.0]$ and σ, referred to as the straggle, satisfies $\sigma \in [.50, 5.0]$. The boundary value problem for the potential in the mid-channel region in equilibrium from (3.1a) is

$$w_{xx} = \frac{1}{\lambda}\left(e^{w\ln\lambda} - e^{-w\ln\lambda}\right) + d(x), \tag{4.1}$$

with boundary conditions

$$w(0) = w_s(\bar{v}_{gs}) \quad \text{and} \quad \lim_{x\to\infty} w(x) = -\frac{1}{\ln\lambda}\sinh^{-1}\left(\frac{\beta\lambda}{2}\right).$$

The asymptotic boundary condition for the potential can be imposed at $x = x^*$. The $w_s = w_s(\bar{v}_{gs})$ relationship will be derived later.

As a remark on the boundary condition at the interface, the strategy is to solve (4.1) asymptotically for various ranges of w_s, thereby deriving explicit expressions for $w_x(0)$ as a function of w_s. Finally, using the mixed boundary condition that holds on the interface (2.6), expressions for $\bar{v}_{gs}$ as a function of w_s for various ranges of w_s are obtained. Inverting these relationships gives w_s, and thus the potential, as a function of $\bar{v}_{gs}$ in various gate bias regimes.

The operating regime of the device is characterized by the different dominant balances in the Poisson equation (4.1) in the limit $\lambda \gg 1$ that can hold near the interface. These different balances lead to substantially different behavior in the mobile charge as a function of the gate voltage in the on and off states of the device.

The classification scheme shown below is based on the magnitude of the surface potential w_s. Since for $w_s > -1$, the potential is a decreasing function of x, the value

of w_s determines the importance of the electron concentration $e^{(w-1)\ln\lambda}$ to the space charge density near the interface. If the electron concentration dominates the impurity concentration near $x=0$, the surface is said to be inverted and a thin layer, called an inversion layer, is present near the interface. With these considerations, the following classification, for constant doping $\beta=1$, is normally made:

$$w_s(\bar{v}_{gs})>1 \quad \text{strong inversion},$$

$$0\leqq w_s(\bar{v}_{gs})\leqq 1 \quad \text{weak inversion},$$

$$-1+O(1/\ln\lambda)\ll w_s(\bar{v}_{gs})<0 \quad \text{depletion},$$

$$|w_s(\bar{v}_{gs})+1|=O(1/\ln\lambda) \quad \text{near flatband},$$

$$w_s(\bar{v}_{gs})\ll -1+O(1/\ln\lambda) \quad \text{accumulation}.$$

Notice from (2.6), $\bar{v}_{gs}\approx 0$ at flatband where $w_s=-1$. We analyze below the basic regimes relevant to an n-channel device, namely strong and weak inversion, as well as depletion. The asymptotic potential for the remaining two regimes can be constructed in a similar manner.

The conventional modeling approach valid for constant doping, $\beta=1$, is based on the first integral of (4.1). Although this approach is useful for finding the total charge, it does not provide a simple pointwise description of the potential and, more importantly, is not applicable to the case of variable implants. The asymptotic approach presented below does not suffer from these limitations. However, to illustrate the matching technique we first consider the constant doping case in both weak and strong inversion.

4.1. Weak inversion–depletion ($-1+O(1/\ln\lambda)\ll w_s\leqq 1$). In this case, the dominant contribution to the space charge density near the interface arises from the immobile acceptor ions. The analysis of the matching for this case closely parallels that of Please [10].

Near the interface, the nonlinearity in the Poisson equation can be neglected for $\ln\lambda\gg 1$. The potential near the interface, referred to as the depletion layer potential, w_d, satisfying $w_d(0)=w_s$ is expanded as

$$w_d=\frac{1}{2}x^2+ax+w_s \quad \text{where } a=\sum_{i=0}^{\infty} a_i(\ln\lambda)^{-i},$$

with a_i to be determined. Moreover, in the bulk an expansion of the boundary condition at infinity for $\ln\lambda\gg 1$ provides $w_b=-1+O(1/\lambda^2\ln\lambda)$. Since $w_b\approx -1$ we know that the term $e^{-(w+1)\ln\lambda}$ in (4.1) must become significant for some x. Therefore, the depletion layer potential must be matched to the bulk potential w_b by constructing an internal layer about some unknown depth x_d where the hole and impurity concentrations in (4.1) balance. Matching the solutions in the transition and depletion layers will then determine both x_d, referred to as the depletion width, and a.

An important feature of the matching is to obtain the $(w_s+1-1/\ln\lambda)^{1/2}$ terms that appear in the exact solution. The presence of these terms requires an infinite order expansion of a and x_d in powers of $1/\ln\lambda$ in the asymptotic solution. For $\ln\lambda$ very large, matching only a finite number of such terms results in an accurate asymptotic solution except near flatband. However, for doping levels of $\lambda\approx 10^6$, we have $\ln\lambda\approx 13.8$ and so to retain high accuracy in our asymptotic expansions in weak inversion we will construct an infinite order expansion in powers of $1/\ln\lambda$.

In the transition layer, inspection of (4.1) shows that the appropriate scalings are

$$x_t = (x - x_d)(\ln \lambda)^{1/2} \quad \text{and} \quad w = w_t(x_t) = -1 + h_0(x_t)/\ln \lambda.$$

In terms of these new variables, the transition layer equation for h_0 is

$$h_0'' = 1 - e^{-h_0}, \tag{4.2}$$

where $h_0(\infty) = 0$ is needed to match to the bulk. It is not possible to integrate (4.2) explicitly; a first integral, however, provides the implicit expression

$$-\sqrt{2}x_t = \int_1^{h_0} (e^{-y} + y - 1)^{-1/2}\, dy. \tag{4.3}$$

The lower limit of the integral can be chosen arbitrarily since $O(1)$ changes in its value are reflected in $O((\ln \lambda))^{-1/2}$ changes in the depletion width.

Even though the transition layer solution is not known explicitly, all we require for matching are the asymptotics out of this layer. Defining an intermediate variable x_η via

$$x_\eta = \frac{x - x_d}{\eta(\lambda)} \qquad \text{where} \quad \frac{1}{(\ln \lambda)^{1/2}} \ll \eta(\lambda) \ll 1,$$

and expanding the implicit transition layer solution (4.3) as $x_t \to -\infty$, or alternatively as $h_0 \to \infty$, provides

$$w_t \sim -1 + \frac{1}{2}x_\eta^2 \eta^2 - \frac{x_\eta \eta c}{\sqrt{2}}(\ln \lambda)^{-1/2} + \left(\frac{c^2}{4} + 1\right)(\ln \lambda)^{-1},$$

where

$$c = \int_1^{\infty} [(y-1)^{-1/2} - (e^{-y} + y - 1)^{-1/2}]\, dy. \tag{4.4}$$

The value of c to five significant digits from numerical integration is $c = .81785$.

Similarly, expanding the depletion layer potential in terms of an intermediate variable gives

$$w_d \sim \tfrac{1}{2}x_d^2 + a x_d + w_s + x_\eta \eta (a + x_d) + \tfrac{1}{2}x_\eta^2 \eta^2.$$

To match, we must also expand the depletion width as

$$x_d = \sum_{i=0}^{\infty} x_{di} (\ln \lambda)^{-i/2}$$

and equate powers of $\eta(\lambda)$ in the above expressions. Matching the transition and depletion layer potentials to an infinite order in $O(1/\ln \lambda)$ by solving the resulting algebraic equations gives

$$\begin{aligned} a &= -\sqrt{2}(w_s + 1 - 1/\ln \lambda)^{1/2}, \\ x_d &= -\frac{c}{\sqrt{2}}(\ln \lambda)^{-1/2} + \sqrt{2}(w_s + 1 - 1/\ln \lambda)^{1/2}, \end{aligned} \tag{4.5}$$

of which the first few terms for $\ln \lambda \gg 1$ are

$$a \sim -\sqrt{2}(w_s + 1)^{1/2}\left[1 - \frac{1}{2(w_s+1)\ln \lambda} + \cdots\right],$$

$$x_d \sim \frac{c}{\sqrt{2}}(\ln \lambda)^{-1/2} + \sqrt{2}(w_s + 1)^{1/2}\left[1 - \frac{1}{2(w_s+1)\ln \lambda} + \cdots\right].$$

The leading order term in this expansion is equivalent to the conventional depletion layer approximation, (see Sze [12]), in which the transition layer is neglected and the leading order potential is patched for C^1 continuity to the bulk at some unknown location. Using the expression for a, the depletion layer potential is

$$w_d = \tfrac{1}{2}x^2 - \sqrt{2}(w_s + 1 - 1/\ln\lambda)^{1/2} + w_s.$$

From this expression we notice that the expansion breaks down near flatband where $w_s = -1 + O(1/\ln\lambda)$. When this occurs the transition layer equation is valid up to the interface as there is no region of depleted carriers.

To determine the current flow in § 5 below, the amount of mobile charge from (4.6) in equilibrium defined by

$$Q_c \equiv -\left(\frac{\ln\lambda}{\lambda}\right)^{1/2} \int_0^{x^*} e^{w(\zeta)\ln\lambda}\, d\zeta \tag{4.6}$$

must be evaluated asymptotically for $\ln\lambda \gg 1$ using the depletion layer potential. Since the dominant contribution to Q_c arises from the interface, a two-term expansion from integration by parts provides

$$Q_c \sim -\frac{e^{w_s\ln\lambda}}{\sqrt{2}(\lambda\ln\lambda)^{1/2}(w_s+1-1/\ln\lambda)^{1/2}}\left(1+\frac{1}{2(w_s+1-1/\ln\lambda)\ln\lambda}\right), \tag{4.7}$$

for $\ln\lambda \gg 1$ and $-1 + O(1/\ln\lambda) \ll w_s \leqq 1$. From this expression we note that if $w_s \leqq 0$ there are virtually no mobile carriers near the interface available for current conduction. Alternatively if $w_s > 0$ there are some mobile carriers near the interface that are responsible for a leakage or subthreshold current upon application of a source-drain bias.

For variable doping, $0 < \beta \leqq 1$, a similar analysis applies, although the equations for the matching parameters must be solved numerically. In addition, for variable doping the matching can only be done to leading order. The details of the calculation are provided in Ward [13]. The main assumption needed is that the doping profile is slowly varying in the bulk. For the variable doping case, the leading order (in $1/\ln\lambda$) potential, w_d, in the depletion layer is

$$w_d = w_s + ax + \frac{\beta}{2}x^2 + (1-\beta)\int_0^x (x-\zeta)\, e^{-(\zeta/\sigma)^2}\, d\zeta,$$

where $a = w_d'(0)$, proportional to the total charge, is to be found by matching. Matching the depletion layer and bulk potentials by means of a transition layer, described above, determines a and x_d. To leading order, and using the Gaussian form of the doping profile $d(x)$, we obtain

$$1 + w_s = \int_0^{x_d} \zeta d(\zeta)\, d\zeta,$$

$$a = -\beta x_d - (1-\beta)\int_0^{x_d} e^{-(\zeta/\sigma)^2}\, d\zeta.$$

The implicit expression for the depletion width is easily solved by Newton iterations. As in the case of constant doping, the expression for the asymptotic mobile charge from (4.6) in the variable doping case can be written. We find

$$Q_c \sim \frac{e^{w_s\ln\lambda}}{(\lambda\ln\lambda)^{1/2}a}\left(1+\frac{1}{a^2\ln\lambda}\right). \tag{4.8}$$

We now consider the case of strong inversion characterized by a different dominant balance in the Poisson equation for $\ln\lambda \gg 1$ near the interface. An analogue of this interface layer is not present for p-n junctions unless the junction is strongly one-sided.

4.2. Strong inversion ($w_s \gtrsim 1$). In this case, since $w_s \gtrsim 1$ we have $e^{(w-1)\ln\lambda} \gg 1$ near the interface which results in the potential having a large gradient near $x=0$. In this thin inversion layer the contribution to the space charge density is dominated by the n-carriers. A schematic plot of the potential in strong inversion, illustrating the layer structure for $\ln\lambda \gg 1$, is shown in Fig. 2. To illustrate the matching we again first consider the case of constant doping, $d=1$.

In the inversion layer the appropriate scaling is

$$\tilde{x} = x/\nu(\lambda) \quad \text{and} \quad w_i(\tilde{x}) = w(\tilde{x}/\ln\lambda) = w_{i0}(\tilde{x},\lambda) + \frac{1}{(\ln\lambda)^2} w_{i1}(\tilde{x},\lambda) + \cdots .$$

Substituting this expansion into (4.1) then yields the layer equations

$$w_{i0}'' = \frac{1}{\lambda(\ln\lambda)^2} e^{w_{i0}\ln\lambda} \qquad w_{i0}(0) = w_s, \tag{4.9a}$$

$$w_{i1}'' - \left[\frac{1}{\lambda\ln\lambda} e^{w_{i0}\ln\lambda}\right] w_{i1} = 1 \qquad w_{i1}(0) = 0. \tag{4.9b}$$

There are several solutions to (4.9a) which satisfy the boundary condition on $x=0$. The appropriate solution required for the matching, which satisfies the boundary condition on $x=0$, is

$$w_{i0}(\tilde{x}) = 1 + \frac{1}{\ln\lambda}\ln(\alpha_0^2\ln\lambda) - \frac{2}{\ln\lambda}\ln\left(\sinh\left(\frac{\alpha_o}{\sqrt{2}}\tilde{x} + \gamma\right)\right), \tag{4.10}$$

where

$$\gamma = \sinh^{-1}(\alpha) \quad \text{and} \quad \alpha = \lambda^{(1-w_s)/2}(\ln\lambda)^{1/2}\alpha_0. \tag{4.11}$$

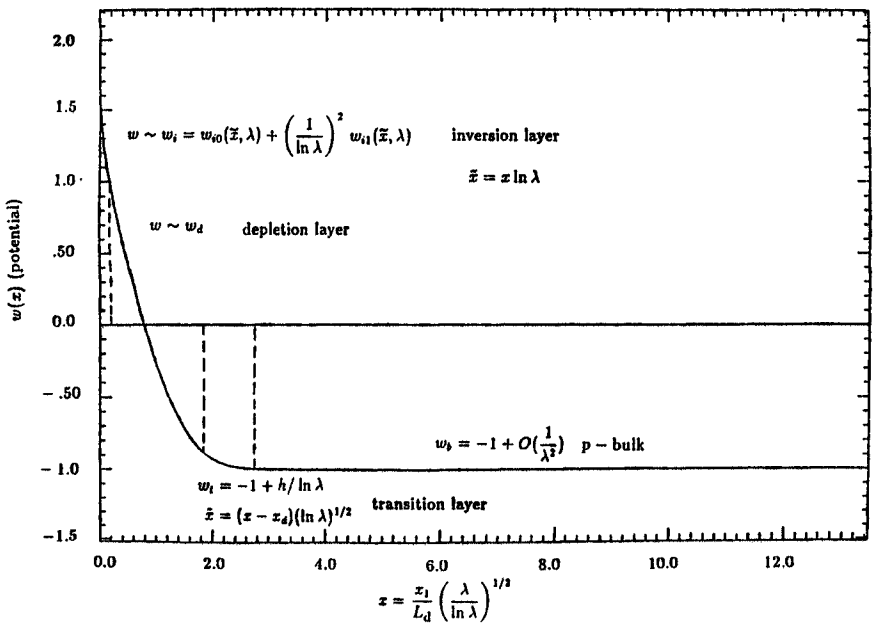

FIG. 2. *Schematic plot of the equilibrium potential.*

The unknown constant $\alpha_0 = O(1)$ will be found by matching. Notice that γ is transcendentally small unless w_s is very near 1.

Defining an intermediate variable x_η by $x_\eta = x/\eta(\lambda)$, where $1/\ln\lambda \ll \eta(\lambda) \ll 1$, then as $\tilde{x} \to \infty$ out of the inversion layer, we have

$$w_{i0} \sim 1 + \frac{\ln(\ln\lambda)}{\ln\lambda} + \frac{2}{\ln\lambda}(\ln(2\alpha_0) - \gamma) - \sqrt{2}\alpha_0 \eta x_\eta. \tag{4.12}$$

As a remark, the equation for the higher order correction w_{i1} from (4.9b), can be solved explicitly using the form of w_{i0}. However, it suffices for matching to obtain the behavior of w_{i1} as $\tilde{x} \to \infty$. A simple calculation shows that

$$w_{i1} \sim \tfrac{1}{2}\tilde{x}^2 + a_{i1}\tilde{x} + b_{i1} \quad \text{as } \tilde{x} \to \infty, \tag{4.13}$$

where, without loss of generality, we can set $a_{i1}, b_{i1} = 0$. Therefore, using the expansions of w_{i0} and w_{i1} we have

$$w \sim 1 + \frac{\ln(\ln\lambda)}{\ln\lambda} + \frac{2}{\ln\lambda}(\ln(2\alpha_0) - \gamma) - \sqrt{2}\alpha_0 \eta x_\eta + \frac{1}{2}x_\eta^2 \eta^2, \tag{4.14}$$

out of the inversion layer.

Since the potential is decreasing, adjacent to the inversion layer we have a depletion layer in which the electron concentration is now subdominant to the impurity concentration. In this region the nonlinear terms in the Poisson equation (4.1) can be neglected, and so with $w_{xx} = 1$ we have

$$w \sim w_d = \tfrac{1}{2}x^2 + ax + b,$$

where $a(\lambda), b(\lambda) = O(1)$ are to be found by matching. Matching the depletion layer to the bulk by means of a transition layer centered at some unknown depth x_d gives a relation for a and x_d in terms of b. A similar calculation as in weak inversion provides

$$\begin{aligned} a &= -\sqrt{2}(b + 1 - 1/\ln\lambda)^{1/2}, \\ x_d &= -\frac{c}{\sqrt{2}}(\ln\lambda)^{-1/2} + \sqrt{2}(b + 1 - 1/\ln\lambda)^{1/2}, \end{aligned} \tag{4.15}$$

with c given by (4.4). Now, in contrast to weak inversion, b is not determined by satisfying the boundary condition on the interface, but rather is found by matching to the inversion layer.

Finally, matching to the inversion layer determines b and α_0. In terms of an intermediate variable, x_η, we have

$$w_d \sim b + a x_\eta \eta + \tfrac{1}{2}x_\eta^2 \eta^2, \tag{4.16}$$

so that matching (4.16) and (4.14) we obtain

$$\begin{aligned} b &= 1 + \frac{\ln(\ln\lambda)}{\ln\lambda} + \frac{2}{\ln\lambda}(\ln(2\alpha_0) - \gamma), \\ \alpha_0 &= (b + 1 - 1/\ln\lambda)^{1/2}, \end{aligned} \tag{4.17}$$

where γ is given by (4.11). Defining K by

$$K(\lambda, w_s, \alpha_0) \equiv \frac{\ln(\ln\lambda)}{\ln\lambda} + \frac{2}{\ln\lambda}[\ln(2\alpha_0) - \gamma] \tag{4.18}$$

and combining (4.17) gives a weakly nonlinear equation for α_0

$$\alpha_0 = (2 + K(\lambda, w_s, \alpha_0) - 1/\ln\lambda)^{1/2}. \tag{4.19}$$

The above equation can be solved approximately or numerically by iteration for fixed large doping levels. Once α_0 is found, the "switchback" term $K(\lambda, w_s, \alpha_0)$ is known and thus x_d, a and b are determined from (4.15), (4.17). Note that, even though $K \ll 1$ for $\lambda \gg 1$, the approximation $\alpha_0 = \sqrt{2}$ is rather poor, since $K \approx .20$ for $\lambda = 10^6$.

An important point to notice is that the order of $K(\lambda, w_s, \alpha_0)$ in the depletion layer expansion depends on the surface potential. In very strong inversion, typically when $w_s \gg 1 + \ln(\ln\lambda)/\ln\lambda$, α is transcendentally small in $\ln\lambda$ as $\lambda \to \infty$. This implies that in this regime, $K(\lambda, w_s, \alpha_0) = O(\ln(\ln\lambda)/\ln\lambda)$ so that the matching parameters α_0, a and the depletion width are highly insensitive to the surface potential w_s. Therefore, for this range of surface potential $\alpha_0 \sim (2 + \ln(\ln\lambda)/\ln\lambda - 1/\ln\lambda)^{1/2}$. However, for $w_s \to 1^+$ the expansion $\sinh^{-1}(\alpha) \sim \ln(2\alpha) + 1/4\alpha^2$ for $\alpha \gg 1$ applies and consequently $K \sim (1/\ln\lambda)^2$. Therefore, in this limit $a \sim (2 - 1/\ln\lambda)^{1/2}$, which agrees asymptotically with the weak inversion result (4.5) when $w_s = 1$.

To compare our asymptotics with the numerical solution to (4.1), the BVP is solved numerically by finite differences on a stretched mesh with the boundary condition as $x \to \infty$ imposed at a few depletion widths from the interface. From Fig. 3, the error defined as the magnitude of the difference between the numerical and asymptotic potential for $\lambda = 10^6$ is roughly .60 percent in both weak and strong inversion.

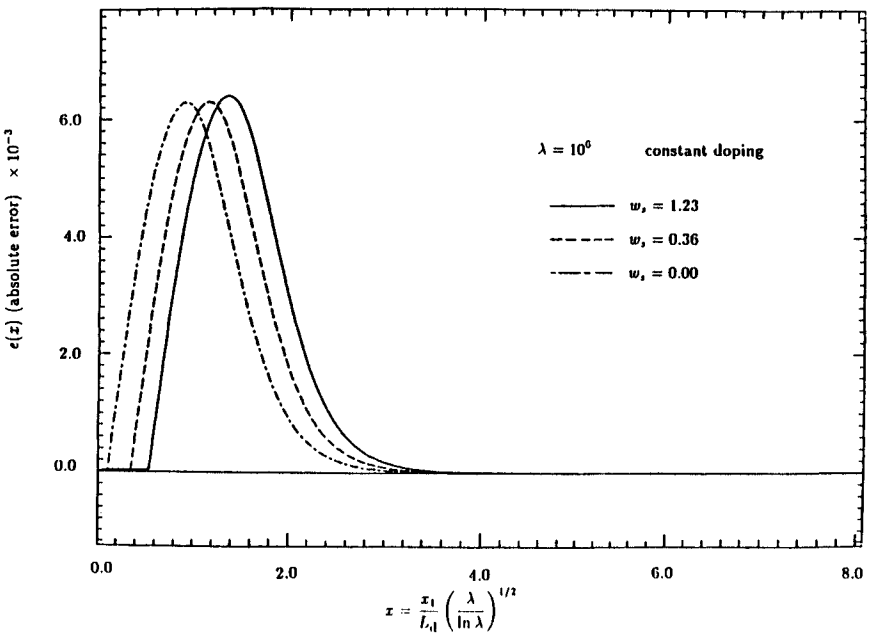

FIG. 3. *Comparison of the asymptotic and the numerical potential.*

Finally, a similar analysis applies for the variable doping case provided the doping is locally constant in the inversion layer and is slowly varying in the bulk. Retaining the same notation for the depletion layer potential as in weak inversion, and after some algebraic manipulations, the coupled leading order equations for the matching

constants are found to be

$$\frac{\beta}{2}x_d^2 + I_2(x_d) = 2 + K(\lambda, w_s, \alpha_0), \tag{4.20a}$$

$$\beta x_d - \sqrt{2}\alpha_0 + I_1(x_d) = 0, \tag{4.20b}$$

where $a = -\sqrt{2}\alpha_0$ and the integrals I_1 and I_2 are defined by

$$I_1(x_d) = \int_0^{x_d} (d(\zeta) - \beta)\, d\zeta \quad \text{and} \quad I_2(x_d) = \int_0^{x_d} \zeta(d(\zeta) - \beta)\, d\zeta. \tag{4.21}$$

For fixed large λ, standard numerical methods are then employed to solve for the matching constants. Further details on the variable doping case are provided in Ward [13].

As a preliminary calculation for obtaining the I-V characteristics in the linear and saturation regime in § 6, the mobile charge Q_c must be computed asymptotically. In this case the dominant contribution to the integral, (4.6), defining Q_c, also arises from the interface. However, using the leading order inversion layer potential constructed in this section, we see that Laplace's method is not directly applicable since the "higher order" terms satisfies

$$\frac{w_{i0}''(0)}{\ln \lambda w_{i0}'(0)^2} = \frac{1}{2(1+\alpha^2)} = O(1) \quad \text{for } \alpha \ll 1.$$

The failure of a routine application of Laplace's method is a result of the strong dependence of the slope of w_{i0} on λ and the near logarithmic singularity of the inversion layer potential at $\tilde{x} = -\sqrt{2}\gamma/\alpha_0 \ll 1$ just outside the domain. To remedy this situation, we evaluate the integral asymptotically by integrating over the inversion layer from the interface to infinity in the stretched variable $\tilde{x}$. Using w_{i0}, the mobile charge integral is given asymptotically by

$$Q_c \sim -(\lambda \ln \lambda)^{1/2} \int_0^{\infty} \frac{1}{\sinh^2(\alpha_0 \tilde{x}/\sqrt{2} + \gamma)}\, d\tilde{x}.$$

A direct computation of this integral provides

$$Q_c \sim -\sqrt{2}\, e^{w_s \ln \lambda/2}(\sqrt{1+\alpha^2} - \alpha), \tag{4.22}$$

where α is given by (4.11) and α_0 in the constant and variable doping cases is found from (4.19) and (4.20a), (4.20b), respectively. This expression for the mobile charge reduces for $\ln \lambda \gg 1$ to the leading order term of the expression for the mobile charge in weak inversion at the strong-weak inversion transition, $w_s = 1$.

Finally, the surface potential is related to the input gate voltage by studying the boundary condition (2.6) that holds on the interface in the mid-channel region. Defining the total charge Q_s by

$$Q_s \equiv -(\lambda \ln \lambda)^{1/2} \int_0^{\infty} w''(x)\, dx = (\lambda \ln \lambda)^{1/2} w'(0),$$

the boundary condition on $x = 0$ from (2.6) becomes

$$F(w_s, \bar{v}_{gs}) \equiv (w_s + 1) \ln \lambda - \frac{Q_s(w_s)}{c_{ox}} - \bar{v}_{gs} = 0. \tag{4.23}$$

From the asymptotic potential for constant doping, we have

$$Q_s \sim -\sqrt{2} \begin{cases} e^{w_s \ln \lambda/2}(1+\alpha^2)^{1/2} & w_s \geqq 1 \\ (\lambda \ln \lambda)^{1/2}(w_s + 1 - 1/\ln \lambda)^{1/2} & -1 + O(1/\ln \lambda) \ll w_s \leqq 1, \end{cases}$$

where α is given by (4.11). The above expressions agree asymptotically at $w_s = 1$. A similar relationship can also be written for the variable doping case. We find

$$Q_s \sim -\begin{cases} \sqrt{2}\, e^{w_s \ln\lambda/2}(1+\alpha^2)^{1/2} & w_s \geqq 1 \\ (\lambda \ln\lambda)^{1/2}\left(\beta x_d + \dfrac{\sigma\sqrt{\pi}}{2}(1-\beta)\operatorname{erf}(\chi_d/\sigma)\right) & -1+O(\ln\beta/\ln\lambda) \ll w_s \leqq 1, \end{cases}$$

where α and x_d are given by (4.11) and (4.20a), (4.20b), respectively. Since the total charge is known in both weak and strong inversion as a function of w_s, (4.23) is easily inverted for $w_s = w_s(\bar{v}_{gs})$ by Newton iterations. In the case of variable doping, an inner Newton iteration cycle is needed to solve for the matching parameters at each step of the outer iteration.

For constant doping a first integral of (4.1) exists, and using the asymptotic boundary condition for the potential, the total charge is

$$Q_{sc}(w_s) \sim -\sqrt{2}(e^{w_s \ln\lambda} + e^{-w_s \ln\lambda} + w_s \lambda \ln\lambda + \lambda(\ln\lambda - 1))^{1/2}.$$

As discussed earlier, the first integral only exists for the case of constant doping. The asymptotic analysis presented above gives the total charge under both constant and variable doping. To check the accuracy of the asymptotics we now compare the asymptotic total charge with the total charge obtained from the first integral assuming constant doping. The total charge as a function of the gate voltage for constant doping as obtained from both the first integral and the asymptotic theory is compared in Fig. 4 where the relative error is plotted. The two expressions are seen to be in very close agreement under both weak and strong inversion.

A plot of the surface potential as a function of the gate voltage for variable doping using the asymptotic total charge is shown in Fig. 5. Using the $w_s = w_s(\bar{v}_{gs})$ relationship and the expressions for the mobile charge in weak and strong inversion under variable doping, the mobile charge as a function of the gate voltage is plotted in Fig. 6. The critical voltage, $\bar{v}_{gsth}$, which we define as the value of the gate voltage where $w_s = 1 + \ln(\ln\lambda)/\ln\lambda$, is labeled on the graph. This definition is motivated by the fact that

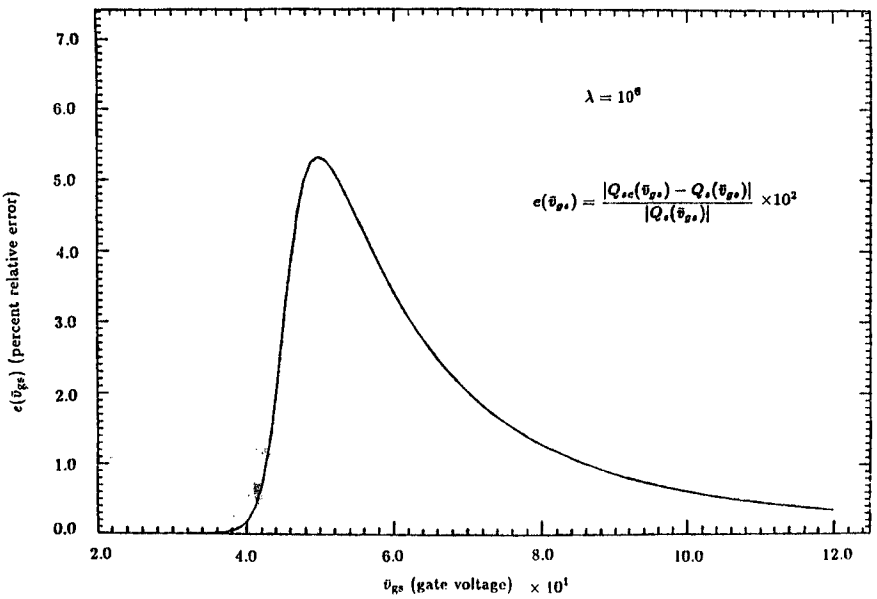

FIG. 4. *Comparison of the total charge.*

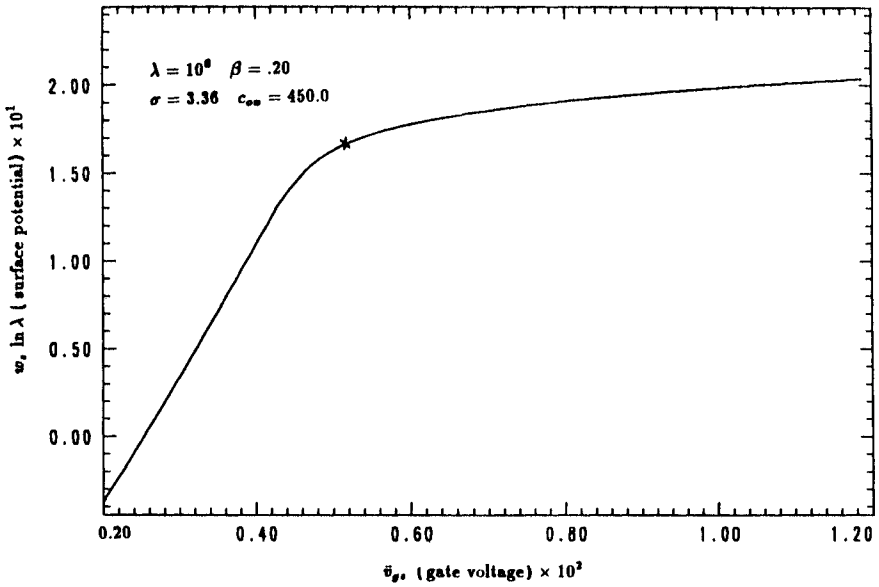

FIG. 5. *Surface potential as a function of the gate voltage.*

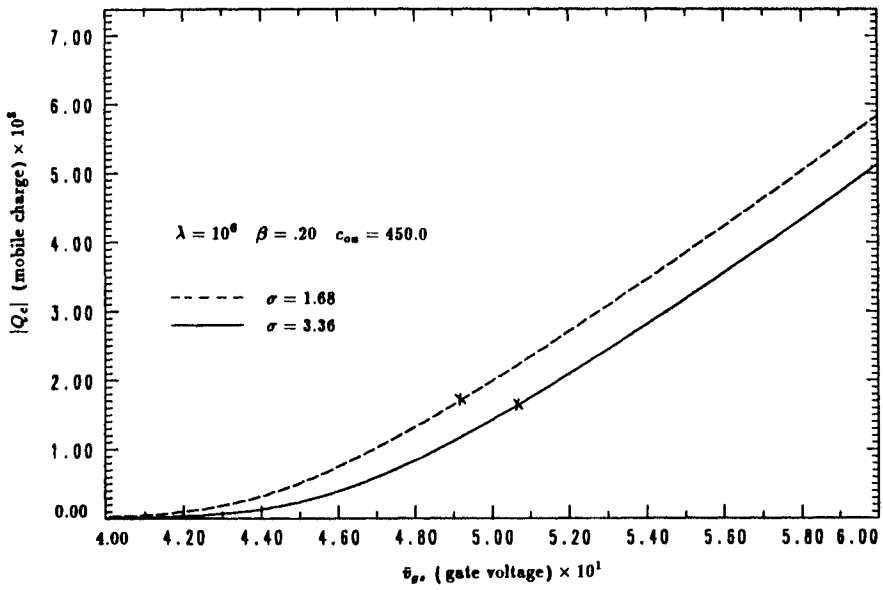

FIG. 6. *Mobile charge as a function of the gate voltage.*

the critical parameter α, and hence the mobile charge, changes its behavior at $\bar{v}_{gsth}$. From this figure we notice that once strong inversion conditions have been established, further increases in the gate voltage are reflected almost exclusively in the buildup of mobile charge near the interface.

An important consequence of the detailed analysis of the equilibrium potential in the $\lambda \gg 1$ limit is that the total and mobile charges are easily evaluated asymptotically in all bias regimes. This feature allows for current-voltage relations that agree asymptotically across the boundary between weak and strong inversion. The analysis of the

nonequilibrium problem that follows relies strongly on the asymptotic results derived for the equilibrium problem. We now derive the current-voltage relations for the subthreshold current flow.

5. Subthreshold current flow. In the subthreshold case, corresponding to the weak inversion regime, there is a small leakage current upon application of a source-drain bias. In this case the gate voltage is sufficiently low so that the contribution to the space charge density of the mobile n-carriers can be neglected for $\lambda \gg 1$ near $y = O(\varepsilon)$ where $\phi^0 \approx 0$. Since $\phi^{'0} > 0$ in the channel, the contribution to the space charge density of the mobile n-carriers can be neglected everywhere in the mid-channel region. This implies that the nonequilibrium potential from (3.1a) is independent of $\phi^0(y)$ for $\lambda \gg 1$ and consequently is given asymptotically by the equilibrium potential in weak inversion. Since the surface potential is also independent of y in the channel, then for constant mobility (3.3) reduces asymptotically to

$$\phi^{''0} - \ln \lambda (\phi^{'0})^2 = 0, \tag{5.1}$$

in the mid-channel region. Neglecting the transverse electric field in the inner regions near the source and drain, the boundary conditions (2.4a) are imposed on (5.1) and thus

$$\phi^0 = -\frac{1}{\ln \lambda} \ln (1 - (1 - \exp(-\bar{v}_{ds}))y).$$

Since asymptotically there is no transverse electric field in the mid-channel region, the current flow is due to diffusion. Using the definition of the current, (2.8), with $\mu = 1$ and the mobile charge, (4.6), we find

$$I_{ds} \sim -I_c (1 - \exp(-\bar{v}_{ds})) Q_c(w_s(\bar{v}_{gs})).$$

Using the asymptotic results (4.8) for the mobile charge in weak inversion, the current-voltage relation is given by

$$I_{ds} \sim I_c \frac{(1 - e^{-\bar{v}_{ds}})\, e^{w_s \ln \lambda}}{(\lambda \ln \lambda)^{1/2} |a|} \left(1 + \frac{1}{a^2 \ln \lambda}\right) \quad \text{as } \lambda \to \infty, \quad \varepsilon \to 0,$$

where $a = a(\bar{v}_{gs})$ is given by (4.5) and (4.20a), (4.20b) under constant and variable doping, respectively. The $w_s = w_s(\bar{v}_{gs})$ relationship is determined from (4.23) using the asymptotic total charge. The leading order term under constant doping is in agreement with the result by Barron [1] based on conventional device modeling.

A plot of the current versus the source-drain bias for various gate voltages under variable doping is shown in Fig. 7. Due to the exponential dependence of the current on the surface potential, small increases in the gate voltage are reflected in relatively large increases in the current. A plot of the current versus the source-drain bias for fixed gate voltage and for various straggles σ of the variable implant is shown in Fig. 8. Since, as seen in Fig. 6, the amount of mobile charge in equilibrium is smaller for larger straggles, the leakage current under subthreshold conditions is also smaller for larger straggles.

Next, we consider the case when the dominant contribution to the space charge density arises from the mobile n-carriers near the interface in some region of the channel.

6. The linear and saturation regimes. In this section the MOSFET is analyzed when the dominant contribution for $\lambda \gg 1$ to the space charge density near the interface arises from the mobile n-carriers in some region of the channel. It is assumed that at an $O(\varepsilon)$ distance away from the source, where $\phi^0 = 0$, the gate voltage exceeds threshold. The threshold voltage here is defined as the value of the gate voltage in

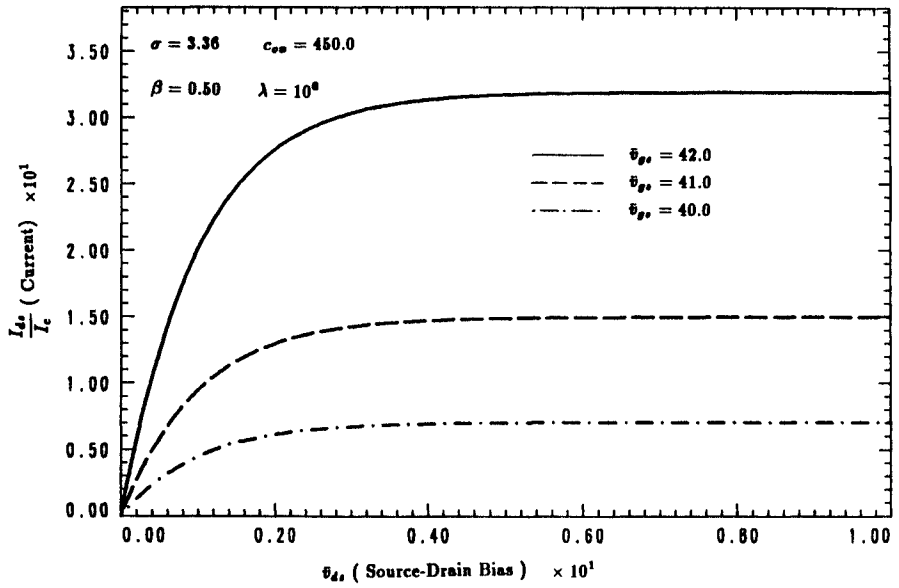

FIG. 7. *Current versus drain bias in weak inversion for various gate voltages.*

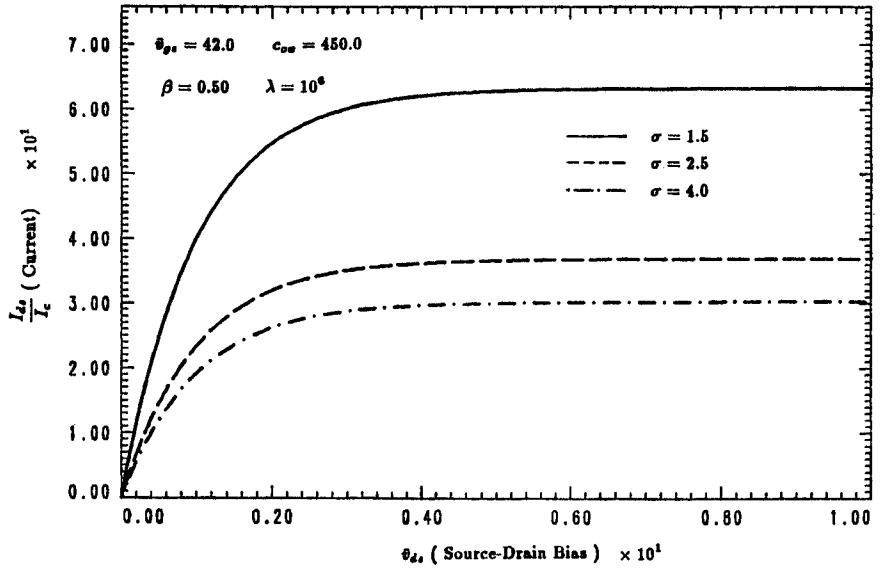

FIG. 8. *Current versus drain bias in weak inversion for various straggles.*

equilibrium for which $w_s = 1$. Therefore, for some region of the channel an inversion layer exists and the mobile electrons drift under the influence of the transverse electric field toward the drain. Depending on the relative magnitude of the gate voltage and the source-drain bias, the inversion layer may extend throughout the channel up to an $O(\varepsilon)$ distance away from the drain. This range of gate voltage and source-drain bias constitute the linear regime. For other ranges of gate voltage and source-drain bias the dominant balance for $\lambda \gg 1$ near the interface in the Poisson equation changes at some position y^* in the channel referred to as the pinchoff position. For $y > y^*$ the

dominant contribution to the space charge density arises from the fixed impurity ions as the mobile n-carriers are now subdominant near the interface. In this post-pinchoff region, which is typically quite narrow, the flow of current will be seen to be primarily due to diffusion. This range of gate voltage and source-drain bias constitute the saturation regime. In this section we will determine the electron concentration and the potential throughout the channel in both the linear and saturation regimes under constant mobility but will allow for variable doping. The current-voltage relations associated with these regimes will also be determined.

Before discussing pinchoff in detail, the potential in the inversion layer from (3.1a) for $\lambda \gg 1$ with ϕ^0 as parameter can easily be constructed using the asymptotic theory presented in § 4. Assuming $w_s - \phi^0 > 1$ near the source, so that a local inversion layer exists, the potential in this layer for $\lambda \gg 1$ retaining the same notation as in § 4, is

$$w_{i0}(\tilde{x}) = 1 + \phi^0 + \frac{\ln(\ln\lambda)}{\ln\lambda} + \frac{2}{\ln\lambda}\ln(\alpha_0) - \frac{2}{\ln\lambda}\ln\left(\sinh\left(\frac{\alpha_0\tilde{x}}{\sqrt{2}} + \gamma\right)\right), \tag{6.1}$$

where $\tilde{x} = x\ln\lambda$. We have dropped the superscript (0) for the potential since only the leading order term in the expansion for ε will be considered. Matching to the depletion layer in the usual way determines both α_0 and the depletion width x_d. Retaining the same notation as in § 4, we find for constant doping

$$x_d = \sqrt{2}(2 + \phi^0 + K(\lambda, w_s, \alpha_0, \phi^0) - 1/\ln\lambda)^{1/2}, \tag{6.2a}$$

$$\alpha_0 = (2 + \phi^0 + K(\lambda, w_s, \alpha_0, \phi^0) - 1/\ln\lambda)^{1/2}, \tag{6.2b}$$

where

$$K(\lambda, w_s, \alpha_0, \phi^0) = \frac{\ln(\ln\lambda)}{\ln\lambda} + \frac{2}{\ln\lambda}[\ln(2\alpha_0) - \gamma], \tag{6.3a}$$

$$\alpha = \alpha_0(\ln\lambda)^{1/2}\lambda^{(1-w_s+\phi^0)/2} \quad \text{and} \quad \gamma = \sinh^{-1}(\alpha). \tag{6.3b}$$

For variable doping, the leading order coupled system of algebraic equations for x_d and α_0 are analogous to those in (4.20a), (4.20b). The coupled equations are

$$\frac{\beta}{2}x_d^2 + I_2(x_d) = 2 + K(\lambda, w_s, \alpha_0, \phi^0), \tag{6.4a}$$

$$\beta x_d - \sqrt{2}\alpha_0 + I_1(x_d) = 0, \tag{6.4b}$$

where the integrals I_1 and I_2 are defined in (4.21). Once the variation of ϕ^0 with y has been determined from the differential equation resulting from the Fredholm alternative condition (3.5), the asymptotic potential in the mid-channel region is known explicitly in terms of x and y.

For fixed gate voltage, the minimum source-drain bias such that pinchoff occurs at the end of the channel can easily be found from the depletion approximation. By definition, pinchoff occurs at the end of the channel when the dominant balance there for $\ln\lambda \gg 1$ changes between weak and strong inversion, i.e.,

$$w_s - \phi^0 = 1 \quad \text{at } y = 1 - O(\varepsilon) \quad \text{where } \phi^0 = \bar{v}_{ds}/\ln\lambda.$$

Using the mixed boundary condition for the potential that holds along the interface, (2.6), combined with the potential in weak inversion, the pinchoff curve in the $(\bar{v}_{gs}, \bar{v}_{ds})$ plane for constant doping is

$$\bar{v}_{gs} = 2\ln\lambda + \bar{v}_{ds} + \frac{\sqrt{2\lambda}}{c_{ox}}(2\ln\lambda + \bar{v}_{ds} - 1)^{1/2}.$$

This curve delineates the boundary between the linear and saturation regimes as shown in Fig. 9. A similar relationship can also be found for variable doping.

As a first step in determining the current, we notice that for constant mobility, $\mu \equiv 1$, (3.5) reduces to

$$\ln \lambda \phi'^0 \, e^{-\phi^0 \ln \lambda} \int_0^{x^*} e^{w^0 \ln \lambda} \, dx \sim \frac{I_{ds}}{I_c} \left(\frac{\lambda}{\ln \lambda} \right)^{1/2}. \tag{6.5}$$

As in § 4, equation (4.22), the integral appearing above can be computed asymptotically for $\lambda \gg 1$ using the parameterized potential w^0 in the inversion layer (6.1). Provided an inversion exists, i.e., $w_s - \phi^0 > 1$, we have

$$\left(\frac{\ln \lambda}{\lambda} \right)^{1/2} \int_0^{x^*} e^{w^0 \ln \lambda} \, dx \sim \sqrt{2} \, e^{(w_s + \phi^0) \ln \lambda / 2} [(1+\alpha^2)^{1/2} - \alpha], \tag{6.6}$$

where α is given (6.3b). In the linear regime this expression is valid throughout the channel. However, in the saturation regime, the above expression does not apply throughout the channel since we have $w_{sp} \equiv w_s(y^*) = 1 + \phi^0(y^*)$ for some $y^* \in (0, 1)$. At the pinchoff position y^*, $\alpha = \alpha_0 (\ln \lambda)^{1/2} \gg 1$ and thus using $(1+\alpha^2)^{1/2} - \alpha \sim 1/2\alpha$, and assuming constant doping, (6.6) reduces to

$$\left(\frac{\ln \lambda}{\lambda} \right)^{1/2} \int_0^{x^*} e^{w^0 \ln \lambda} \, dx \sim \frac{e^{w_{sp} \ln \lambda}}{\sqrt{2 \lambda \ln \lambda} (1 + w_{sp} - 1/\ln \lambda)^{1/2}} \tag{6.7}$$

in the post-pinchoff region $y > y^*$. Since in this post-pinchoff region the asymptotic potential for $\lambda \gg 1$ is independent of y, the differential equation for ϕ^0 given by (6.5) in this region is identical to that studied in the subthreshold regime. Therefore, in the region $y^* < y < 1 - O(\varepsilon)$ the flow of current is due to diffusion.

A significant complication in the analysis arises from the nonnegligible transverse electric field established in the oxide as a result of the bias applied on the drain contact. This field implies that the surface potential along the interface varies with the position

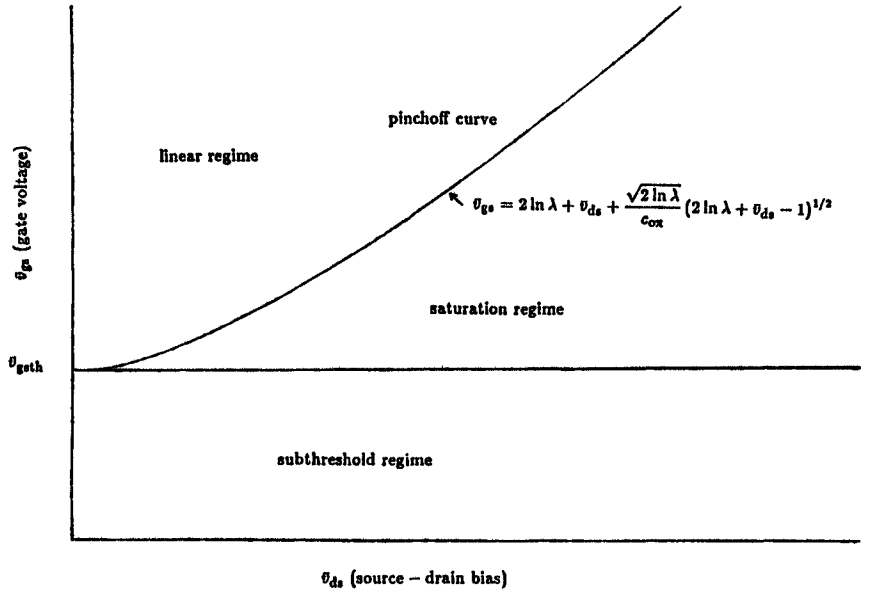

FIG. 9. *Control plane illustrating the various bias regimes.*

y along the channel in the linear regime. The transverse electric field results in a drift component to the current density parallel to the interface. To determine the variation of w_s with y along the channel, we must first examine the mixed boundary condition for the potential that holds along the interface. For constant doping we also compare our $\lambda \gg 1$ results with those predicted by conventional modeling based on a first integral of (3.1a) with ϕ^0 as parameter. The mixed boundary condition (2.6) from § 2 for fixed $\bar{v}_{gs}$ is

$$F(w_s, \phi^0) \equiv (w_s + 1) \ln \lambda - \frac{Q_s(w_s, \phi^0)}{c_{ox}} - \bar{v}_{gs} = 0, \tag{6.8}$$

where the total charge $Q_s = Q_s(w_s, \phi^0)$, for constant doping, satisfies

$$Q_s \sim -\sqrt{2} \begin{cases} e^{(w_s - \phi^0)\ln\lambda/2}(1+\alpha^2)^{1/2} & \text{asymptotic,} \\ (e^{(w_s-\phi^0)\ln\lambda} + e^{-w_s \ln\lambda} + w_s \lambda \ln \lambda + \lambda (\ln \lambda - 1))^{1/2} & \text{conventional,} \end{cases}$$

and α given by (6.3b). The asymptotic total charge is valid provided that an inversion layer exists, i.e., $w_s - \phi^0 > 1$. Once the pinchoff condition $w_s - \phi^0 = 1$ for some y^* has been attained, the expression for the total charge in weak inversion is used in (6.8).

To compare the asymptotic and conventional expressions for the charge, for a given $\bar{v}_{gs}$, (6.8) can be solved numerically by Newton's method for $w_s = w_s(\phi^0)$. As in the case when $\phi \equiv 0$ from Fig. 3, the agreement between the asymptotic and the conventional theories is found to be excellent. As before, the asymptotic approach allows for an easy examination of the variable doping case. In all computations that follow, the asymptotic total charge under both constant and variable doping is used.

We now solve the coupled system (6.5), (6.8) for ϕ^0 and $w_s(y)$ and determine the current I_{ds} subject to the boundary conditions $\phi^0(0) = 0$ and $\phi^0(1) = \bar{v}_{ds}/\ln \lambda$ in both the linear and saturation regimes.

Since $\phi^{0\prime} > 0$ it is convenient to consider $y = y(\phi^0)$ where from (6.5)

$$I_{ds} y'(\phi^0) = -I_c Q_c(w_s(\phi^0), \phi^0) \ln \lambda. \tag{6.9}$$

As shown above, the mobile charge Q_c is known asymptotically for $\ln \lambda \gg 1$ in the channel in both the linear and the saturation regimes. Since the derivative of F with respect to w does not vanish, the implicit function theorem shows that the surface potential $w_s = w_s(\phi^0)$ can be found from (6.8) using the asymptotic total charge Q_s, i.e., $F(w_s(\phi^0), \phi^0) = 0$.

The source-drain current is then found by integrating (6.9) from $\phi^0 \ln \lambda = 0$ to $\phi^0 \ln \lambda = \bar{v}_{ds}$;

$$I_{ds} = -I_c \int_0^{\bar{v}_{ds}} Q_c(w_s(u/\ln \lambda), u/\ln \lambda)\, du, \tag{6.10}$$

where we use the asymptotic expressions for the mobile charge. The electron quasi-Fermi potential ϕ^0 is then found from the implicit relationship

$$I_{ds} y = -I_c \int_0^{\phi^0} Q_c(w_s(\eta), \eta) \ln \lambda \, d\eta. \tag{6.11}$$

These integrals are evaluated by Simpson's rule as a function of the source-drain bias for various gate voltages. A plot of the current versus source-drain bias for constant channel doping and for various $\bar{v}_{gs}$ is shown in Fig. 10. From this figure we notice that as the gate voltage increases the current saturates at larger source-drain biases. The current voltage relations for various straggles σ in the variable implant are shown in

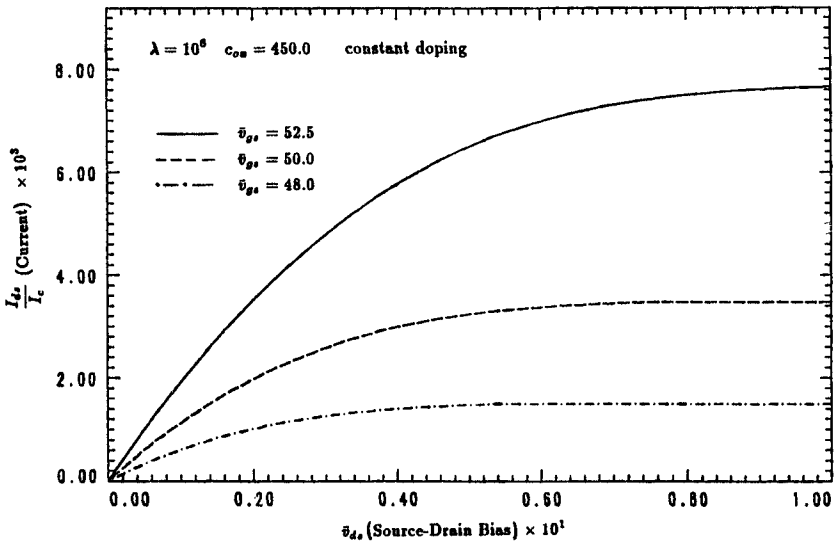

FIG. 10. *Current versus drain bias for constant doping in saturation regime.*

Fig. 11. It is seen that the current-voltage relations in the linear regime are relatively insensitive to variations in the straggle. On the other hand, the saturation behavior, e.g., the dependence of the saturation current on the gate voltage, depends strongly on the parameters characterizing the channel implant.

It is important to emphasize that the pinchoff position y^* in the channel is quite insensitive to source-drain biases in the saturation regime. This is due to the fact that the current increases only marginally once saturation has occurred, since then the dominant contribution to the mobile charge integral arises from those electrons closer to the source. Thus, the pinchoff position $y^* < y < 1 - O(\varepsilon)$ is in general quite thin.

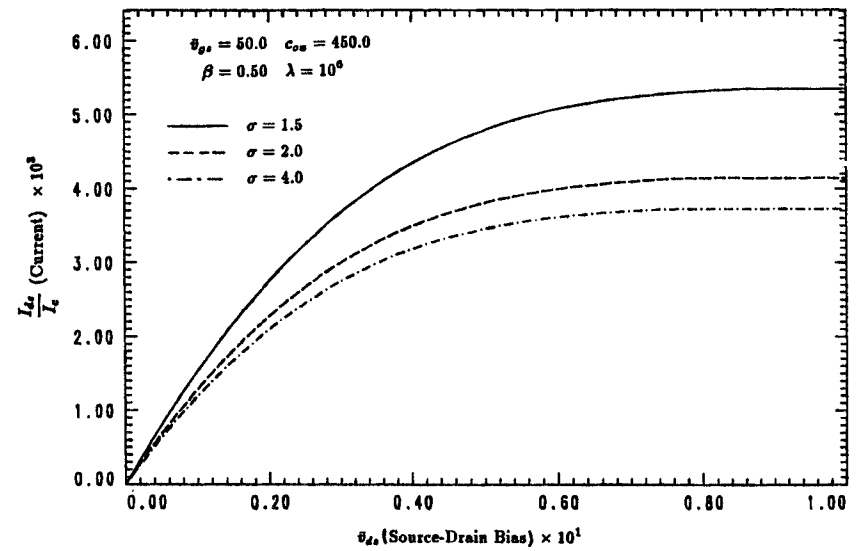

FIG. 11. *Current versus drain bias for variable doping in saturation regime.*

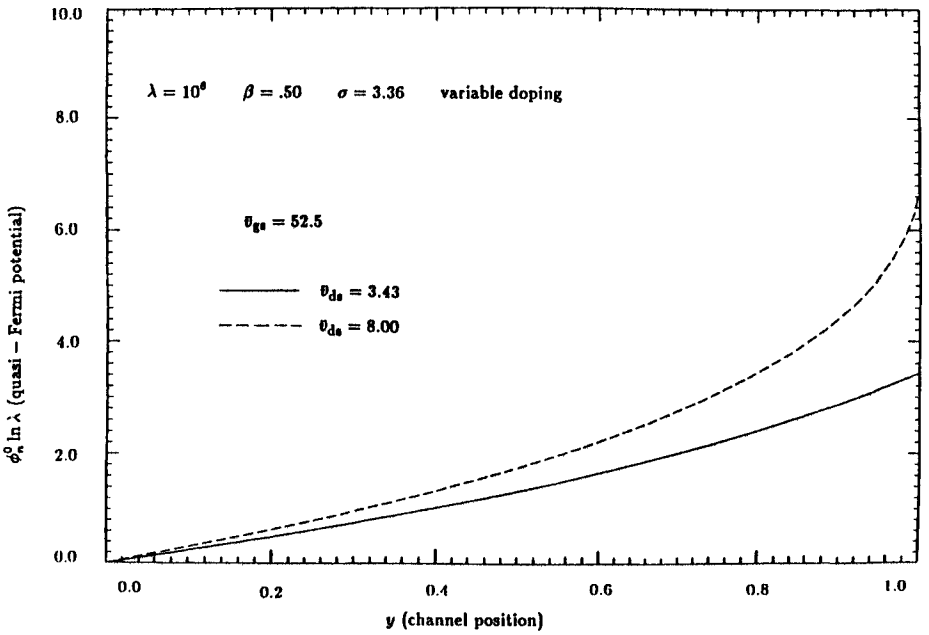

FIG. 12. *Electron quasi-fermi potential for various drain biases.*

Using the two relations (6.10) and (6.11), ϕ^0 can be found numerically as a function of y in the channel. A plot of the electron quasi-Fermi potential in the channel for various $\bar{v}_{ds}$ is shown in Fig. 12. The logarithmic singularity in the electron quasi-Fermi potential just outside the domain, that was found in the subthreshold case, is also apparent in this case as well. Finally, with ϕ^0 known, the surface potential $w_s(y)$ and hence the parameterized potential $w^0(x, y)$ is known as a function of position in the region $O(\varepsilon) < y < 1 - O(\varepsilon)$.

Acknowledgments. The authors acknowledge preliminary calculations, related to some of the material of § 4, by L. Reyna and H. Cohen.

REFERENCES

[1] M. BARRON, *Low level currents in insulated gate field effect transistors*, Solid State Electronics, 15 (1972), pp. 293-302.

[2] J. BREWS, *Physics of the* MOS *transistor*, Applied Solid State Supplement 2A, Academic Press, New York, 1981.

[3] ———, *A charge-sheet model of the* MOSFET, Solid State Electronics, 21 (1978), pp. 344-355.

[4] W. FICHTNER, D. ROSE, AND R. BANK, *Semiconductor device simulation*, SIAM J. Sci. Statist. Comp., 4 (1983), pp. 391-415.

[5] J. GREENFIELD, *Analysis of intrinsic* MOS *devices and parasitic effects using solutions of Poisson's equation*, Ph.D. thesis, Stanford Electronics Lab, Stanford, CA, 1982.

[6] J. KERVORKIAN AND J. COLE, *Perturbation Methods in Applied Mathematics*, Springer Verlag, Berlin, New York, 1981.

[7] P. MARKOWICH, *A singular perturbation analysis of the fundamental semiconductor device equations*, SIAM J. Appl. Math., 44 (1984), pp. 896-928.

[8] ———, *The Stationary Semiconductor Device Equations*, Springer Verlag, Wien, New York, 1986.

[9] H. PAO AND C. SAH, *Effects of diffusion currents on characteristics of metal-oxide semiconductor transistors*, Solid State Electronics, 9 (1966), pp. 927-937.

[10] C. PLEASE, *An analysis of semiconductor* P-N *junctions*, IMA J. Appl. Math., 28 (1982), pp. 301–318.
[11] S. SELBERHERR, *Analysis and simulation of semiconductor devices*, Springer Verlag, Wien, New York, 1984.
[12] S. SZE, *Physics of semiconductor devices*, John Wiley, New York, 1969.
[13] M. WARD, *Asymptotic methods in semiconductor device modeling*, Ph.D. thesis, Caltech, Pasadena, CA, 1988.